

MODEL-BASED CAVITY SHAPE ESTIMATION IN A GAS-LIQUID SYSTEM WITH NONUNIFORM IMAGE SAMPLING

Magnus Evestedt

Department of Information Technology, Uppsala University
P.O. Box 337, SE-951 05, Sweden

Alexander Medvedev

Department of Information Technology, Uppsala University
P.O. Box 337, SE-951 05, Sweden

Keywords: Image analysis, feature extraction, model-based application, image sampling.

Abstract: A water model is studied to simulate physical phenomena in the Lintz-Donawitz steel converter. The depression in the liquid, due to the impinging gas jet, is measured by means of a video camera. Image processing tools are used to extract the edge of the surface indentation. The measured edge, sampled in a special way, is used together with a nonlinear mathematical model to obtain a description of the cavity profile. The parameters of the mathematical model are optimized to match the registered cavity edge in the image at a set of sampled points. Three ways of choosing sampling points for the optimization are proposed and compared on simulated as well as experimental data. An approach involving an observer decreases the computation time with an acceptable loss of accuracy of the estimates.

1 INTRODUCTION

The properties of a system consisting of a gas jet impinging on a liquid surface from above are important in many industrial applications. The focus of this paper is on a steel making process involving top blowing e.g. the Lintz-Donawitz (LD) converter. It is widely used and stands for 60% of the world steel production, (www.steel.org, 2005).

In the LD converter process, hot metal is converted into steel by a top blown basic oxygen furnace. Scrap and slag forming agents are added to the hot metal before oxygen is blown onto the metal bath, from above, at supersonic speed. A cavity is formed where the oxygen jet hits the bath surface and Fe, Si, Mn and C are oxidized. The jetting also produces large amounts of slag, where most of the chemical reactions take place.

The lance position over the bath, together with the oxygen flow rate are usually used as manipulated variables in the process. A deeper understanding of the system of the gas jet and the liquid surface would improve the efficiency of blowing and the control of the process. The important parameters, determining heat and mass transport at the interface and in the liquid, are the interface shape, the width and depth of the cavity and the height of the peripheral lip, (Eletribi et al., 1997), see Figure 1. The diameter of the lance is de-

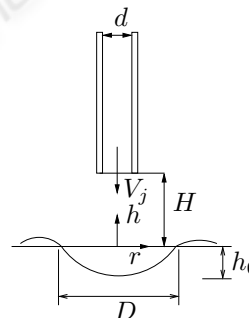


Figure 1: Gas jet impinging on a liquid surface.

noted by d , the maximum velocity of the gas V_j and H is the lance height above the liquid surface. D and h_0 are the diameter and depth, respectively, and h and r define the axes in the coordinate system.

Depending on the properties of the gas jet and the liquid, three modes of surface deformation have been identified in the process: dimpling, splashing and penetrating, (Molloy, 1970). These modes are illustrated in Figure 2. Only the first two modes are considered in the sequel.

Since the form of the cavity is difficult to observe in the actual process, due to the hostile environment, a water model of the LD converter is often used. In the

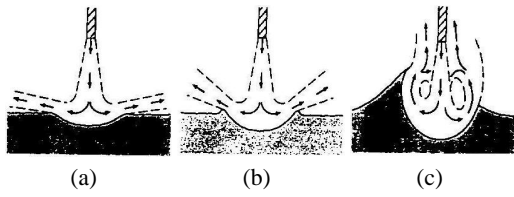


Figure 2: Modes of surface deformation by the impinging gas jet according to (Molloy, 1970). (a) Dimpling, (b) Splashing, (c) Penetrating.

water model the molten steel is replaced by water and compressed air is used instead of oxygen. The similarities between the water bath and the molten steel are analyzed in (Lee et al., 2002).

Energy and force balances were considered in (Rosler and Stewart, 1968), to describe the indentation profile. The results were later used in (Berghmans, 1972), for a study of the stability of interfaces between fluids in motion.

In (Evestedt and Medvedev, 2005) the cavity surface model in (Berghmans, 1972) was used, together with experimental data from a water model, to approximate the surface deformation and to quantify the uncertainty of the depth and diameter estimates. The uncertainty was shown to decrease when the temporal dynamics of the cavity were modelled as a sum of sine waves.

In this paper a sampling algorithm to improve the efficiency of the estimation procedure in (Evestedt and Medvedev, 2005) is given. The paper is organized as follows: First a system model is introduced. Then three approaches to choosing sampling points for the optimization are presented, followed by a description of the experimental setup. The paper is concluded with a comparison between the methods using both simulated and experimental data.

2 PROBLEM FORMULATION

In (Berghmans, 1972) a mathematical model for the gas-jet system was suggested. The model was investigated further in (Evestedt and Medvedev, 2005), where it was reformulated in state-space form as

$$\frac{dx}{dr} = f(r, x) = \begin{bmatrix} x_2 \\ \frac{1}{\sigma}(\Delta p + (\rho_1 - \rho_2)gx_1) [1 + x_2^2]^{\frac{3}{2}} - \frac{\delta}{r}x_2 [1 + x_2^2] \end{bmatrix} \quad (1)$$

$$x = [x_1 \ x_2]^T$$

where $x_1 = h$, $x_2 = \frac{dh}{dr}$, g is the gravitational constant, Δp is the over-pressure due to the impinging jet, $\delta = 1$, ρ_1 and ρ_2 are the densities of the liquid and

the gas, respectively and σ is the surface tension of the specific liquid-gas combination.

To determine Δp , Rosler and Stewart used the experimental data of Gibson, for laminar jets impinging on a flat plate, (Gibson, 1934). The pressure distribution is approximated by:

$$\Delta p = \begin{cases} p_{\max} \cos(0.826 \frac{r}{r_j}) & \text{for } r \leq 1.2r_j \\ 4.53p_{\max} \exp(-1.76 \frac{r}{r_j}) & \text{for } r > 1.2r_j \end{cases}$$

where r_j is the jet radius, $p_{\max} = \frac{1}{2}\rho_1 V_j^2$ is the jet strength and V_j is the maximum jet velocity. In the following, δ , σ and $x_1(0)$ are treated as tuning parameters.

The problem treated in this paper is then to estimate the parameters $\theta = [\delta, \sigma, x_1(0)]$ in (1) from a video sequence showing the liquid formation on the surface of a water tank.

The cavity edge is extracted from the image frames. Each point on the edge is assigned a coordinate (i, j) describing its position in the image. A conversion from the image coordinates (i, j) to actual coordinates $(h(r), r)$ is performed via image calibration. Define a set of coordinates as $M \in R^2$, and N as the number of pixels in the set (cardinal number of M). In (Evestedt and Medvedev, 2005), the following criterion function is used to estimate the parameters in (1) by optimization.

$$\hat{\theta} = \arg \min_{\theta} L(\theta) \quad (2)$$

$$L(\theta) = \frac{1}{N} \sum_{r \in M} (h(r) - \hat{h}(r))^2$$

where $\hat{h}(r)$ is the model output.

The optimization is performed over the set M , using `fminsearch` in Matlab[®]. In the following, the approach in (Evestedt and Medvedev, 2005), where all data points, obtained by edge detection, belong to M , will be referred to as *Scheme 1*.

The underlying algorithm for the multidimensional unconstrained nonlinear minimization is the Nelder-Mead search, (Nelder and Mead, 1965). It is based on evaluating a function at the vertices of a simplex or hypertetrahedron, then iteratively shrinking the simplex as better points are found until some desired bound is achieved. Due to the lack of convergence results, the efficiency and complexity of the Nelder-Mead search algorithm are hard to estimate, (Singer and Singer, 2004). In this particular application, the time needed for the algorithm to converge is dependent on the number and placement of the data used in the parameter tuning.

The contribution of this paper is two model-based approaches to choose the sampling points used in the optimization in such a way that the computation time is substantially decreased, with acceptable reduction of the estimation accuracy.

3 PARAMETER ESTIMATION

In this section, two alternative model-based approaches to decrease the computation time of the optimization, by utilizing the data that contain most information about the edge, are presented. The schemes are based on the vital assumption that the cavity shape does not change abruptly from one frame to another.

3.1 Sampling

The continuous model described by Equation (1) is nonlinear. There is no general theory regarding sampling of nonlinear systems that can be applied directly in this case. Consider a linear second order homogeneous ordinary differential equation, which can be seen as a linearization of (1)

$$y''(t) + ay'(t) + by(t) = 0 \quad (3)$$

where the parameters a and b are constant real coefficients. Let a solution to Equation (3), (cf. Simmons, 1991), be given by

$$y(t) = C_1 e^{\lambda_1 t} + C_2 e^{\lambda_2 t} \quad (4)$$

where λ_1 and λ_2 are negative real numbers and $\lambda_1 \neq \lambda_2$ given by

$$\lambda_{1,2} = -\frac{a}{2} \pm \sqrt{\frac{a^2}{4} - b} \quad (5)$$

In order to obtain a spectrum describing the distribution of energy over frequency, ω , Equation (4) is readily Fourier transformed to obtain

$$|Y(\omega)|^2 = \left| \frac{C_1}{j\omega - \lambda_1} + \frac{C_2}{j\omega - \lambda_2} \right|^2 \quad (6)$$

According to the sampling theorem (cf Oppenheim and Schaffer, 1989), a band-limited signal (*i.e.* one with a zero spectrum for frequencies $\omega > \omega_B$), can be fully reconstructed from its sampled version, if the sampling rate is chosen at least twice as large, that is $2\omega_B$. Normally a much higher sampling rate is recommended, (Åström and Wittenmark, 1997).

As can be seen in Equation (6), the spectrum decreases as $\frac{1}{\omega^2}$. This property holds for all solutions to (3). An important user choice when sampling Equation (4) is the threshold, ω_B , above which the energy content in the signal can be considered so small that it can be neglected. The reconstruction accuracy is of course highly dependent upon this choice.

The frequency content of the solution to the nonlinear Equation (1) is more difficult to characterize. Here, a special feature is utilized, namely the fact that the second state describes the derivative of the indentation profile. Thus, it provides information on how fast the curve changes. This property underlies the following sampling methods.

3.2 An Ad-hoc Approach

The most interesting points of the indentation profile are where it changes most rapidly. Studying the derivative of the model adjusted to fit the measurement obtained at time t in Figure 3, it can be seen that the derivative decreases with increasing radial distance r from the origin. The idea is to only use the points where the derivative exceeds a user-defined threshold in the optimization of the model parameters to the measurement obtained at time $t + 1$. Thus the amount of data is reduced, decreasing the computation time.

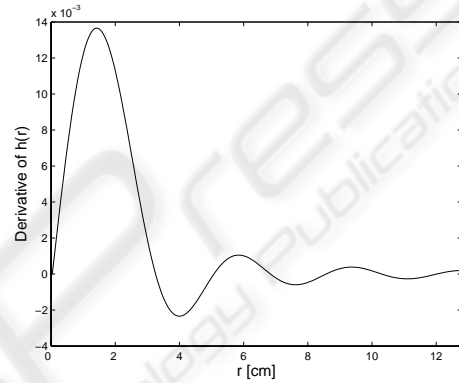


Figure 3: The derivative of the model edge.

A summary of the proposed approach is as follows:

Scheme 2

1. Define a threshold, T , for the derivative of the cavity edge *w.r.t.* r .
2. Take the first frame in the video sequence and extract the edge of the cavity. Let *all* edge pixels constitute the set M . Solve optimization problem (2).
3. Evaluate Equation (1) for the parameters $\hat{\theta}(t)$ obtained in the previous step to estimate the derivative of the cavity edge *w.r.t.* r .
4. Find the pixels where the derivative is larger than a user-defined threshold. Let those points constitute M .
5. Retrieve the next image frame.
6. Detect the cavity edge.
7. Sample the detected edge only at the points in M for the optimization.
8. Solve optimization problem (2) to obtain parameter estimate $\hat{\theta}(t)$.
9. Goto (3).

Scheme 2 is thus model-based, but does not take into account the data extracted from the current image. In the next section a Kalman filter is used to estimate the derivative of the model edge, based on the new measurement, to improve the placing of the sampling points.

3.3 A Kalman Filter Based Observer Approach

In this approach the model of the surface at time t is used together with the new measurement at time $t + 1$ to estimate the derivative of the indentation profile. The estimation is performed using the Kalman filter.

To fit nonlinear system (1) into the Kalman filter framework, it is expanded in first order Taylor series around estimates of $x(r)$. The linearization is as follows

$$f(r, x) \approx f(r, \hat{x}) + F(r)(x - \hat{x}) \quad (7)$$

where

$$F(r) = \left. \frac{\partial f(r, x)}{\partial x} \right|_{x=\hat{x}} \quad (8)$$

$$(9)$$

and the linearized system is

$$\frac{dx}{dr} = F(r)x(r) + u(r) + w(r) \quad (10)$$

$$u(r) = f(r, \hat{x}) - F(r)\hat{x} \quad (11)$$

$$y(r) = x_1 + v(r) \quad (12)$$

where $w(r)$ and $v(r)$ correspond to modelling errors and measurement errors, respectively. It is assumed that $w(r)$ and $v(r)$ are white noise sequences with variances R_1 and R_2 .

Now, the Kalman filter can be used as an observer of the process. The continuous Kalman filter equations are

$$\frac{d\hat{x}}{dr} = F(r)\hat{x} + u(r) + K(r)(y(r) - \hat{x}_1(r)) \quad (13)$$

$$\frac{dP}{dr} = F(r)P(r) + P(r)F^T(r) + R_1 - K(r)R_2K^T(r) \quad (14)$$

$$K(r) = P(r)[1 \ 0]^T R_2^{-1} \quad (15)$$

where $y(r)$ in the correction term of (13) is calculated using linear interpolation between subsequent pixels.

The observer based approach can be summarized as follows:

Scheme 3

1. Define a threshold, T , for the derivative of the cavity edge *w.r.t.* r .

2. Take the first frame in the video sequence and extract the edge of the cavity. Let *all* edge pixels constitute the set M . Solve optimization problem (2).
3. Estimate the derivative of the cavity edge *w.r.t.* r from the measurement obtained at time $t + 1$, using the observer (13)-(15) based on the model from time t with the current estimate $\hat{\theta}(t)$.
4. Find the pixels where the derivative estimate is larger than a user-defined threshold. Let those points constitute M .
5. Retrieve the next image frame.
6. Detect the cavity edge.
7. Sample the detected edge only at the points in M for the optimization.
8. Solve optimization problem (2) to obtain parameter estimate $\hat{\theta}(t)$.
9. Goto (3).

4 EXPERIMENTAL SETUP

The experiments in Subsection 5.2 were conducted on a water model of the LD converter, previously used to study and control foaming, (Birk et al., 2003), and to characterize the shape of the cavity, (Evested and Medvedev, 2005). A single hole cylindrical nozzle with diameter 1.5 mm was used. The indentation profile arising when air is jetted onto the liquid surface was recorded using a CCD camera. An example of a photograph taken with the camera together with an approximation of the cavity edge by Equation (1) is shown in Figure 4.

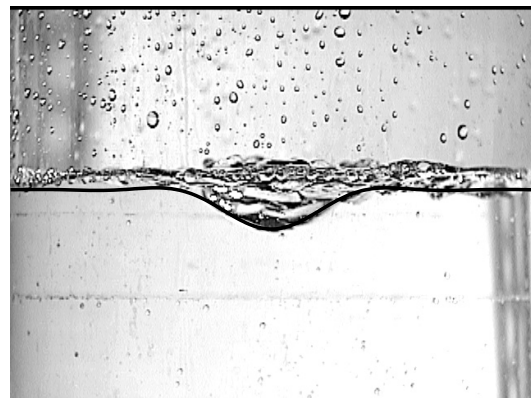


Figure 4: Photograph of the water surface during a blow. An approximation of the cavity edge is included in the image.

4.1 Image Processing

To extract the edges from the photographs an in-house software was used, previously employed in (Evestedt and Medvedev, 2005). The frames of the video sequence are filtered to reduce the noise in the image. Then edge detection is applied using a thresholding method, together with some basic image processing tools such as opening, closing and flood-fill, (Sonka et al., 1999).

4.2 Sources of Error

There are several sources of error in the experimental setup.

- The oxygen flow through the lance is slowly varying with time.
- The lance angle to the water bath cannot be guaranteed to be 90 degrees.
- Bubbles and splashing make the edge detection difficult.

5 RESULTS

In this section the three optimization approaches are compared to each other in terms of approximation accuracy, computation time and data utilization. The comparison is performed on simulated as well as experimental data.

5.1 Simulation Results

A sequence of 50 ideal edges obtained from Equation (1) was used to study the performances of the considered methods. The edge was corrupted using a white sequence to simulate the random error sources. The parameters, θ , were varied in a manner similar to that observed in experiments.

The three optimization schemes were employed to find estimates, $\hat{\theta}$, of the parameters. Since the parameters are not constant, the estimation error $\tilde{\theta}(t) = \theta(t) - \hat{\theta}(t)$ is used as a measure of estimation accuracy. In Table 1 the mean value of the ratio between the estimation error and the true parameter is shown in percent. The mean performance in terms of time and data utilization is shown in Table 2.

As can be seen $x_1(0)$ is accurately estimated for all considered methods. The parameters δ and σ seem to be more difficult to estimate, which is indicated by larger estimation errors. Scheme 3 however, provides estimates of reasonable accuracy compared to Scheme 1. Better accuracy can be obtained by lowering the sampling threshold and thus considering more

Table 1: The estimation accuracy of the considered schemes given as the mean value of the ratio between the estimation errors, $\tilde{\theta}$ and the true parameter values in θ , shown in %.

	Scheme 1	Scheme 2	Scheme 3
$\tilde{\delta}/\delta$	0.38	3.11	1.90
$\tilde{\sigma}/\sigma$	7.09	22.0	12.2
$\tilde{x}_1(0)/x_1(0)$	0.56	0.63	0.63

Table 2: The mean performance in terms of approximation accuracy, time and data utilization for the three approaches. Simulated data.

	Scheme 1	Scheme 2	Scheme 3
Time [s]	16.7	8.97	4.4
Data [%]	100	25	24

edge points in the estimation. The most significant gain of using Scheme 2 over Scheme 1 is in reduction of the optimization time. If Scheme 3 is used instead, the computation time is decreased even further, with higher estimation accuracy compared to Scheme 2. From Table 2 it follows that the computation time using Scheme 3 is just a quarter of the one using Scheme 1.

5.2 Experiments

A sequence of 50 frames was obtained experimentally using the water model setup, with a lance height of 12 cm and a gas flow rate of 21 l/min. Image processing techniques were utilized to obtain the edge of the cavity. The three approaches, Schemes 1, 2 and Scheme 3, were used to approximate the measured edge.

Since true model parameter values are unknown in the experiments, Equation (2) is used as a measure of how well the cavity form is approximated. The full edge measurement is considered as the true edge, $h(r)$, in the loss function $L(\theta)$. In Figure 5, the estimation accuracy of the optimization approaches are shown. As can be seen, the reduction of data points does not significantly affect the accuracy of the approximation, except at the locations of the peaks. It is likely that splashing water in the tank destroys the edge detection and invalidates the model at these points. The best approximation is naturally the approach using all the measured data.

The mean performance in terms of time, approximation accuracy and data utilization is shown in Table 3. The large peaks for some of the edge realizations affect the mean values significantly, explaining the large mean values of $L(\theta)$ in Scheme 2 and Scheme 3.

Table 3: The mean performance in terms of approximation accuracy, time and data utilization for the three approaches. Experimental data.

	Scheme 1	Scheme 2	Scheme 3
L	0.015	13.6	0.41
Time [s]	38.5	33.3	27.4
Data [%]	100	63	61

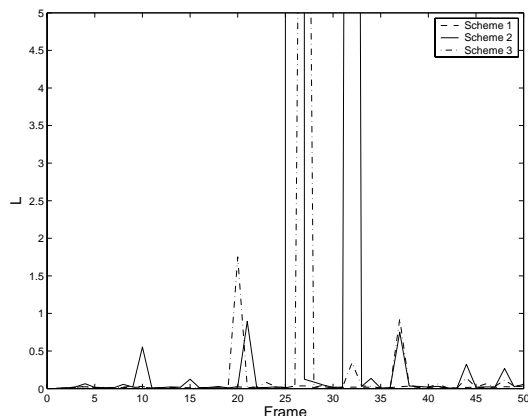


Figure 5: The approximation accuracy for the three optimization approaches using 50 realizations of the edge.

6 CONCLUSIONS

Two approaches to selecting sampling points in a nonuniform way in the images of a surface cavity in a water model were proposed. Instead of using all the data points, a smaller number of data was utilized and shown both on simulated as well as on experimental data to decrease the computation time with an acceptable reduction of the estimation accuracy.

ACKNOWLEDGMENTS

This work has been in part supported by The Swedish Steel Producers' Association and by the EC 6th Framework programme as a Specific Targeted Research or Innovation Project (Contract number NMP2-CT-2003-505467).

REFERENCES

- Berghmans, J. (1972). Theoretical investigation of the interfacial stability of inviscid fluids in motion, considering surface tension. *Journal of Fluid Mechanics*, 54:129–141.
- Birk, W., Arvanitidis, I., Jönsson, P., and Medvedev, A. (2003). Foam level control in a water model of the

LD converter process. *Control Engineering Practice*, 11:49–56.

Eletribi, S., Mukherjee, D. K., and Prasad, V. (1997). Experiments on liquid surface deformation upon impingement by a gas jet. In *Proceedings of the ASME Fluids Engineering Division*, volume 244.

Evestedt, M. and Medvedev, A. (2005). Gas jet impinging on liquid surface: Cavity shape modelling and estimation. In *Proceedings of the 16th IFAC World Congress*.

Gibson, A. H. (1934). *Hydraulics and Its Application*. London:Constable.

Lee, M. S., O'Rourke, S. L., and Molloy, N. A. (2002). Fluid flow and surface waves in the BOF. *ISS Transactions*, 29(10):56–65.

Molloy, N. A. (1970). Impinging jet flow in a two-phase system: the basic flow pattern. *Journal of the iron and steel institute*, pages 943–950.

Nelder, J. A. and Mead, R. (1965). A simplex method for function minimization. *Computer Journal*, 7:308–313.

Oppenheim, A. V. and Schaffer, R. W. (1989). *Discrete-Time Signal Processing*. Prentice Hall.

Rosler, R. S. and Stewart, G. H. (1968). Impingement of gas jets on liquid surfaces. *Journal of Fluid Mechanics*, 31:163–174.

Simmons, G. F. (1991). *Differential equations with applications and historical notes*. McGraw Hill, Inc.

Singer, S. and Singer, S. (2004). Efficient implementation of the Nelder-Mead search algorithm. *Applied Numerical Analysis & Computational Mathematics*, 1:524–534.

Sonka, M., Hlavac, V., and Boyle, R. (1999). *Image processing, analysis and machine vision*. PWS Publishing.

Åström, K. J. and Wittenmark, B. (1997). *Computer-controlled systems*. Prentice Hall.

www.steel.org (2005). Steel industry technology roadmap. www.steel.org.